Nuclear Physics **A452** (1986) 699–722
©North-Holland Publishing Company

THE NUCLEAR LATTICE MODEL OF PROTON-INDUCED MULTI-FRAGMENTATION REACTIONS*

W. BAUER, U. POST, D.R. DEAN and U. MOSEL

Institut für Theoretische Physik, Justus-Liebig-Universität Giessen, D-6300 Giessen, West Germany

Received 16 July 1985
(Revised 12 November 1985)

Abstract: A model of proton-induced multi-fragmentation reactions based on percolation theory is described and applied to experimental data. With only the simplest of assumptions the essential features of the mass-yield curves, such as their U-shape and their power-law dependence for low-to-medium masses, are reproduced. However, the model is, as will be demonstrated, flexible enough to allow for the inclusion of different physical mechanisms. The fits to mass-yield data are then quantitative over the whole mass range. The connection with real physics is made and some relevant experiments are suggested.

1. Introduction

The production of complex fragments in nuclear collisions at intermediate and high energies is a difficult and far-from-understood area of current nuclear physics research. Experiments have been made with both proton and heavy-ion beams and the literature is now extensive [for a review, see e.g. ref. [1])]. Many seemingly different phenomena, such as evaporation, spallation, fission and multi-fragmentation reactions (MFR), have been identified [1]), but in recent years it is the last of these that has received the most attention. This was triggered by the startling suggestion [2]) that MFR are a manifestation of critical behaviour in nuclei.

Properties of infinite nuclear matter [3]) indicate that such a "liquid–gas" phase transition is to be expected and it may be that the physical conditions attainable can probe the relevant region of the nuclear equation of state. Calculations for real, finite nuclei also suggest that some sort of phase instability exists [4,5]). On the other hand, though, investigations of the fragmentation of hot classical drops subject to classical molecular dynamics [6]) suggest that MFR *cannot* be used to study the phase diagram in the region of the critical point. This is because the fragmentation occurs not at the isothermal spinodal, but at the adiabatic one, which, in general, does not extend to temperatures as high as the critical one. Consequently it is by no means certain that the phase-transition model can correctly describe MFR.

* Work supported by BMFT and GSI Darmstadt.

More fundamental criticisms can also be made of the critical-behaviour approach. Is thermalization of the system possible in the short time available, for example? Why do so many different experiments give similar results, despite the fact that macroscopic phase transitions are notoriously difficult to study in detail? And, at an even more fundamental level, can such behaviour be invoked for a very small system where the high charge density almost certainly plays an important role? After all, many standard thermodynamic arguments lose their validity in the presence of long-range forces[7]), a problem discussed in detail by Thirring[7]). Questions such as these cast doubt on the applicability of standard thermodynamics to the problem at hand.

These criticisms have led to other, more conservative descriptions of multi-fragmentation reactions. Sequential evaporation has been extended to higher excitation energies[8]) and is useful for obtaining some information on the time development of the system. Initially the system is supposed to be in a state of thermal equilibrium and the evaporation is a surface phenomenon. However, TDHF-based approaches[9]) suggest that multi-fragmentation occurs throughout the volume of the system, but such calculations suffer from, amongst other things, problems in the description of the collision phase.

Phase-space calculations with thermodynamical input have also been made[10-12]), whereas other authors make statistical assumptions which lead to a description of MFR as a shattering[13]) or a percolation-like[14]) process.

The maximum entropy formalism has been used to show that the available MFR data contain rather little physical information[15,16]). This approach resembles standard percolation theory (SPT)[17]), insofar that both provide the statistically most favoured state. Deviations of the experimental results from these predictions give a clue to the true physics of MFR, but these are unfortunately small.

In view of the many different models used and assumptions made in the study of MFR, we felt that it would be useful to have *one* method which could be used in a flexible manner to test *various* physical assumptions. To this end we proposed the nuclear lattice model (NLM)[18]). In its simplest form the nucleons are taken to occupy the sites of a three-dimensional simple-cubic lattice. Neighbouring pairs of sites are connected initially by bonds. Some bonds are then broken in a model-dependent manner and the size distribution of connected nucleons (which we call "clusters" and identify with nuclei) is evaluated. We explain the details of the NLM in sect. 2, where we also discuss its similarity to and differences from standard percolation theory.

With such a flexible model the effects of various assumptions can be studied. Breaking the bonds in a random, uniform way corresponds to a purely statistical break-up, which in some ways can be associated with the multi-fragmentation of a thermalized system. As we show in sect. 3 this approximation describes the general features of the mass-yield data quite well, but improvements can be made, as we also describe in that section. In sect. 4 we consider other observables, in particular the multiplicity distributions.

Of course, the NLM is a crude approximation of reality and some justification of it is necessary, as is the physics of the bond breaking. These points are covered in sect. 5. We note also that both proton and heavy-ion beams are used to study MFR and it is not yet clear that the physical mechanisms are the same. In principle the NLM can be used for both types of projectile, but proton-induced reactions are more amenable to a first application of the model, in view of the assumptions inherent in it. This point is discussed further in sect. 5 and we end with our conclusions and outlook for future use of the model.

2. Percolation theory and the nuclear lattice model

2.1. PERCOLATION THEORY FOR FINITE SYSTEMS

Any percolation model has two crucial ingredients: a description of the distribution of a set of points or sites in a given d-dimensional space, and a criterion for deciding whether two given points or sites are connected. Connected sites are said to form clusters and by definition there is no path between different clusters. The study of properties of these clusters constitutes percolation theory.

The most easily visualizable percolation model consists of a lattice, the sites of which are occupied at random with a probability p. If p is not too big, only small, isolated clusters are produced, by for $p \to 1$ a cluster extending throughout the whole lattice exists. This is known as the percolating cluster. The fundamental result of percolation theory is that for $p_C \leq p \leq 1$ the percolating cluster occurs with probability one, providing that the lattice is infinite in extent. That is, for $p < p_C$ no percolating cluster exists and for $p \geq p_C$ one *and only one* such cluster is present. The quantity p_C is called the critical occupation probability and the properties of the clusters for p close to p_C are described by scaling theory[17]). We call the above-described model standard percolation theory (SPT), since a lattice is present which is both infinite in extent and occupied randomly.

The results of scaling theory show that only the *dimension* of the lattice plays a role in determining the properties of the clusters close to the percolation threshold. In particular, these properties can be expressed in terms of a few so-called critical exponents, which are purely dimension dependent. For example, as a function of p the number of clusters of size s per lattice site, $n_s(p)$, varies as

$$n_s(p) \propto s^{-\tau} f(s^{\sigma}(p - p_C)), \tag{2.1}$$

where $f(0) = 1$ and τ and σ are critical exponents with values for $d = 3$ of about 2.15 and 0.45, respectively. The so-called scaling function f is discussed in ref.[17]).

The percolation threshold p_C itself depends not only on the dimensionality of a lattice, but also on its particular topology. For the square lattice $p_C \simeq 0.593$, whereas for the simple, body-centred and face-centred cubic lattices $p_C \simeq 0.311$, 0.245 and

0.198, respectively[17]). For simple hypercubic lattices

$$p_C \simeq 1/(2d-1), \tag{2.2}$$

for $d \to \infty$ dimensions. Despite this topological variation, scaling theory shows that the cluster properties of, say, a simple and body-centred cubic lattice will be identical for the same value of $p - p_C$ (see eq. (2.1)).

The sudden appearance of an infinite cluster for $p \geq p_C$ suggests that something rather like a phase transition is occurring. Consequently SPT is used to describe both thermodynamic and magnetic systems undergoing changes of phase. A more exotic application has been made in the study of the quark-gluon plasma[19]) and it can also be applied to more general collective phenomena, polymer gelation and the spread of blight in an orchard.

One might worry that for the study of a gas, for example, the lattice is rather artificial and should be dispensed with. Calculations show, however, that its presence plays a small role and the results for randomly positioned as well as randomly occupied sites differ only slightly from those of SPT[17]).

An intimately related percolation model is that of bond percolation. Instead of the sites being occupied at random, *all* sites are occupied, but the bonds between them are *broken* at random with a breaking probability p_B. The critical breaking probabilities p_{BC} are 0.500 and 0.751 for square and simple-cubic lattices, respectively[17]), and we stress that for $p_B \leq p_{BC}$ the percolating cluster exists, in contrast to the above-described site-percolation problem where it is present for $p \geq p_C$. Otherwise bond percolation can be described in the same way as site percolation and, in many cases, transformations can be made from one to the other[20]). A combination of bond and site percolation has also been constructed[21]) which we are considering as a possible extension of the NLM for the study of heavy-ion induced MFR (see sect. 6).

We take the bond-percolation problem to be the starting point for the NLM description of MFR and our eventual aim is to relate the concept of our bonds, and hence the breaking probability, to the effective nucleon-nucleon interaction. Campi *et al.*[14]) use the site-percolation problem as the basis of their calculations.

The main difference between the NLM and SPT is that the nuclear system is described by a *finite* lattice in order to include important finite-size effects. For such a lattice p_{BC} (and, of course, p_C for the site problem) is no longer well defined, since the percolating cluster can disappear for $p_B < p_{BC}$. In fig. 1 we show as a function of p_B and n the percolation probability P_{perc} defined as the probability with which a single cluster connects two opposite faces of a finite $n \times n \times n$ simple-cubic lattice. As $n \to \infty$ P_{perc} tends to the step function

$$P_{perc} \to \theta(p_{BC} - p_B). \tag{2.3}$$

It is useful to study some properties of these finite-lattice calculations. This we do by evaluating the fractional shift ε and the fractional rounding δ of the distribution

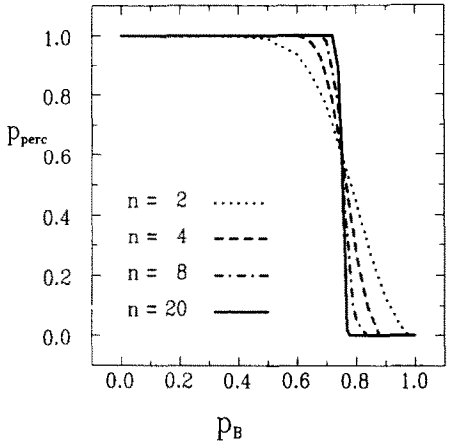

Fig. 1. For various values of n the probability of bond percolation, $P_{perc}(p_B)$, is shown as a function of the breaking probability p_B for $n \times n \times n$ simple-cubic lattices.

$P_{perc}(p_B)$ with respect to the infinite-lattice limit. If p_{B1} and p_{B9} are defined by

$$P_{perc}(p_{B1}) \equiv 0.1, \qquad P_{perc}(p_{B9}) \equiv 0.9, \tag{2.4}$$

and the critical breaking probability $p_{BC}(n)$ for the finite system by that value of the breaking probability for which the absolute value of $dP_{perc}(p_B)/dp_B$ is a maximum, we can write

$$\varepsilon(n) \equiv (p_{BC}(n) - p_{BC}(\infty))/p_{BC}(\infty), \tag{2.5}$$

$$\delta(n) \equiv (p_{B1}(n) - p_{B9}(n))/p_{BC}(\infty). \tag{2.6}$$

In fig. 2 we plot these quantities as functions of n and conclude that

$$\varepsilon(n) \simeq 0.20/n^{0.96}, \tag{2.7}$$

$$\delta(n) \simeq 0.80/n^{1.00}. \tag{2.8}$$

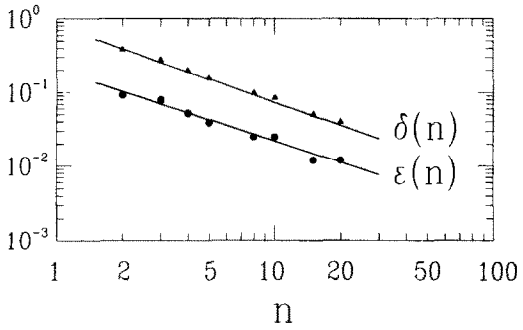

Fig. 2. The fractional shift $\varepsilon(n)$ and fractional rounding $\delta(n)$ as defined by eqs. (2.5) and (2.6), are shown as functions of n for $n \times n \times n$ simple-cubic lattices. The straight lines are the fits of eq. (2.7) and (2.8).

These results should be compared with those presented by Fisher[22]) and Heermann and Stauffer[21]), who show that for large but finite lattices ($10 \leq n \leq 100$) both $\varepsilon(n)$ and $\delta(n)$ are proportional to $1/n^{1/\nu}$, where the critical exponent ν is about 0.88 for $d = 3$ [refs.[17,21,22])].

The calculation of $\varepsilon(n)$ is harder than that of $\delta(n)$ since, as will be shown below, the fluctuations in the fragment yields are largest for $p_B \simeq p_{BC}$. Consequently good statistics are more difficult to obtain. We note, however, that if other definitions of $\varepsilon(n)$ are employed, such as replacing $p_{BC}(n)$ in eq. (2.5) by p_{B1} or p_{B9}, similar results to eq. (2.7) are obtained: $\varepsilon(n) \simeq 0.47/n^{1.01}$ and $\varepsilon(n) \simeq -0.33/n^{0.99}$ with p_{B1} and p_{B9}, respectively.

The finite-lattice result that $P_{perc} < 1$ for breaking probabilities just less than the critical one shows that a finite lattice will begin to break up at a lower value of p_B than in the infinite case. This may be identified tentatively with results for the thermal properties of finite nuclei[3-5]), which show that a phase instability occurs at temperatures less than that expected from infinite nuclear-matter calculations.

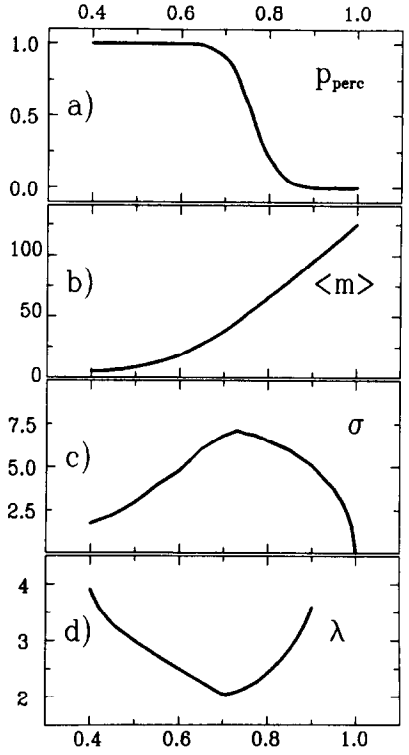

Fig. 3. For a $5 \times 5 \times 5$ simple-cubic lattice the behaviour of (a) $P_{perc}(p_B)$, (b) the mean fragment multiplicity $\langle m \rangle$, (c) the standard deviation of the fragment multiplicity distribution, σ, and (d) the apparent exponent λ are shown as functions of p_B. Correlations between these functions are readily identifiable.

In fig. 3 we show for $n = 5$ how the behaviour of the mean value and standard deviation of the multiplicity distribution are correlated with $P_{\text{perc}}(p_B)$. (The multiplicity is the total number of clusters produced.) Also shown is the p_B dependence of the so-called apparent exponent λ, which, for small fragment size s, is defined by

$$n_s(p_B) = \text{const} \times s^{-\lambda(p_B)}. \tag{2.9}$$

We see that in the critical region λ has a minimum with value equal to the τ of eq. (2.1). This is one of the main "justifications" of the phase-transition model of MFR, since in the droplet theory of Fisher[22]) the yield of droplets of size s varies as $s^{-\tau}$ when the condensation occurs at the fluid's critical point. The large fluctuations in the multiplicity distribution at $p_B \simeq p_{BC}(n)$ are also indications of phase-transition behaviour.

We will return to these results later.

2.2. THE NUCLEAR LATTICE MODEL

Having summarized the mean features of SPT and described the deviations for the case of finite lattices, we now consider in detail the nuclear lattice model (NLM).

We restrict ourselves, as indicated in the introduction, to reactions of the type

$$p + A_T \rightarrow A_F + X, \tag{2.10}$$

and so we distribute the A_T nucleons of the target nucleus in an approximately spherical way over a simple-cubic lattice. We note that arbitrarily deformed nuclei can also be considered, but, providing the "nucleus" is reasonably compact, the results are essentially unchanged. Initially, therefore, each "nucleon" is connected by bonds to a maximum of six nearest neighbours, depending on its location within the "nucleus".

We choose a simple-cubic lattice because it is particularly amenable for computation. As mentioned above, the results of SPT show that only the dimension of the lattice has a marked effect on the cluster properties, with, for a given dimensionality, the particular topology of the lattice determining only the critical occupation or breaking probability. Whereas this can no longer be expected to be true of finite systems, we are not aware of any quantitative results and so we hope that our calculations are reasonably insensitive to the chosen lattice type. We are investigating this point further.

For a given impact parameter b we then remove from the lattice those nucleons in the cylindrical channel with radius r at impact parameter b defined by the fireball geometry (see fig. 4). For proton-induced reactions typically 6–8 nucleons are in the fireball and so the effect on the results is slight, i.e. calculations with and without removing the nucleons in the fireball channel yield very similar results. Therefore, we also obtain nearly the same results for all impact parameters (see subsect. 3.2).

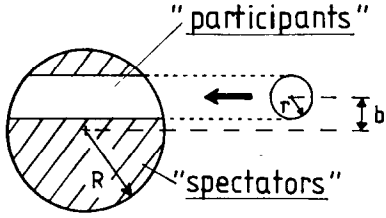

Fig. 4. The fireball geometry: the lattice sites in the cylindrical channel with radius r at impact parameter b are left unoccupied.

Using the breaking probability p_B as an input parameter, a Monte-Carlo algorithm decides for each bond individually whether it is broken or not. This procedure is followed by a counting algorithm which looks for clusters and evaluates their size. The cluster counting is the most time-consuming part of any percolation-like calculation and it is important to have a very efficient algorithm for this purpose. We have developed a technique, described in the appendix, that enables us to perform calculations for a mass-132 lattice in around 8 ms per event on the IBM-3084 at GSI Darmstadt.

Finally we integrate over impact parameter and so obtain complete mass and multiplicity distributions for the prescribed value of p_B. Spin and isospin degeneracy are assumed (but see sect. 6).

It is clear that the only input for a given target mass is p_B, for which different prescriptions can be made in an attempt to study the characteristic features of various physical mechanisms. Herein lies the great strength of our model, since such considerations are not at all possible in other approaches. Physical interpretations of p_B will be given later in the paper.

Before proceeding to a consideration of experimental data, it is worthwhile exploring the simplest properties of the NLM. For this we assume that p_B is the same for each bond, independent of its position on the lattice and of the projectile's impact parameter. For such calculations there is essentially no dependence of the results on the position of the fireball.

In fig. 5 we have chosen $A_T = 132$ ("Xe") and show the behaviour of the fragment-mass distribution for various values of p_B. When p_B is small (0.35) we see that a few nucleons and low-mass fragments are evaporated off, with a large residual nucleus remaining. For high p_B (0.74 and 0.85) no such residual nucleus is present, corresponding to complete break-up of the target.

At intermediate p_B (0.60) we obtain a U-shaped mass distribution. This is a well-known feature of many experimental mass-yield curves. Gross *et al.*[11]) insist that the Coulomb interaction is the main factor responsible for this observation, but we see from our model that such a feature is produced *solely* as a result of the *finite size* of the system.

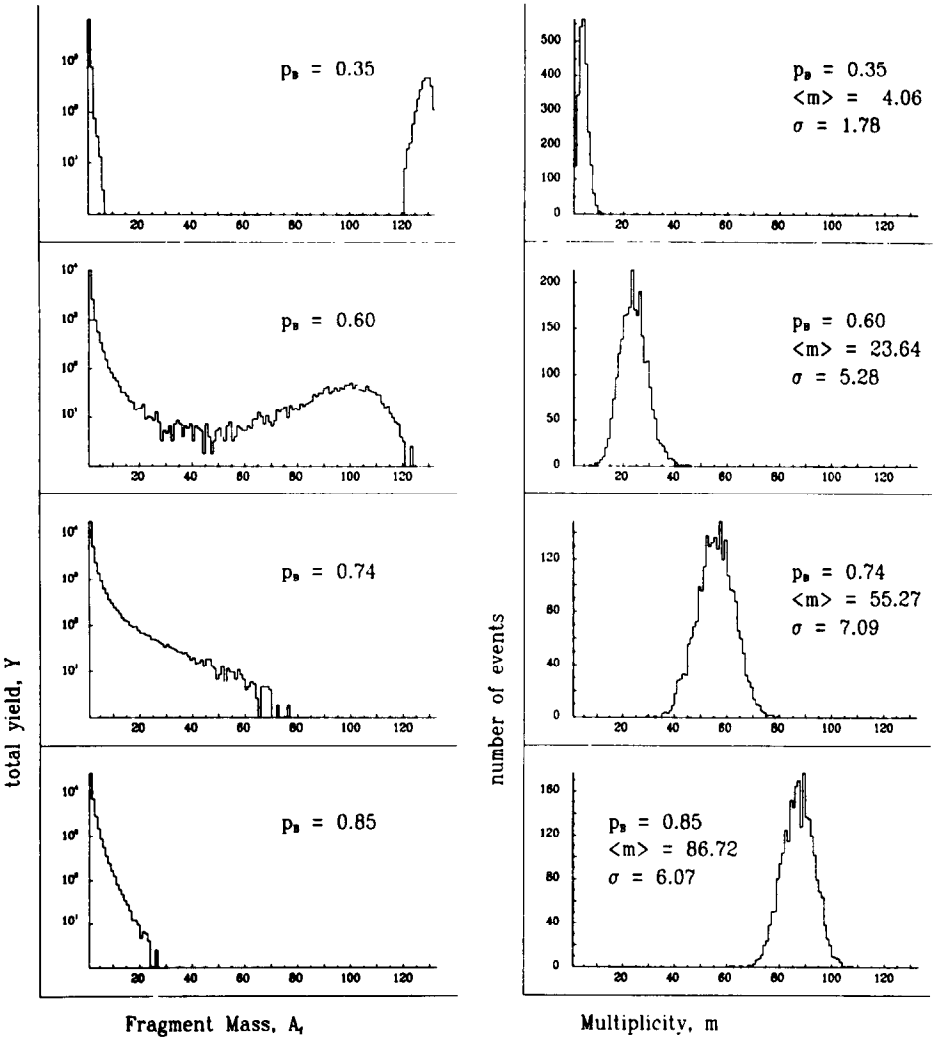

Fig. 5. Dependence of the mass yield (left) and multiplicity distribution (right) on the breaking probability p_B for the reaction p + Xe. Also shown are the mean value $\langle m \rangle$ and the standard deviation σ of the multiplicity distributions. The breaking probability $p_B = 0.74$ is roughly the critical one for this size system.

Also shown in fig. 5 are the multiplicity distributions. The mean multiplicity increases monotonically with increasing p_B, a fact that we will make use of later.

We see from these results that at the critical breaking probability ($p_B = 0.74 \simeq p_{BC}$) the standard deviation of the multiplicity distribution is a maximum, that the mass-yield curve has almost a perfect power-law dependence with $\lambda \simeq 2.21 \simeq \tau$, and that there are no longer any high-mass fragments produced: compare $p_B = 0.60$ and $p_B = 0.74$.

Comparison of experimental data[1,2,23-25]) with the above-described properties of the NLM shows that it is capable of a qualitative description of the available mass-yield curves. We now proceed to show that this description can be made quantitative.

3. Comparison with data

3.1. CALCULATIONS WITH CONSTANT BREAKING PROBABILITY

In the previous section we used a constant breaking probability over the whole lattice to demonstrate that experimental mass-yield curves can be qualitatively described by the NLM. Such a p_B is also used in this section, but we now attempt to make quantitative fits*.

As far as the details of the calculations are concerned, we note that we typically made of the order of 10^4 Monte Carlo runs to obtain mass-yield curves with good statistics.

In fig. 6 we display NLM fits to three sets of experimental data: p + Ag at 11.5 GeV [ref.[23])], p + Ta at 5.7 GeV [ref.[24])] and p + ^{197}Au at 11.5 GeV [ref.[25])]. We see that the general quality of the fits is good, despite the fact that, apart from an overall normalization factor, there is only one free parameter, namely p_B. This is determined with an accuracy of $\Delta p_B \simeq \pm 0.01$ and, interestingly, always takes values of about 0.65, being 0.64, 0.67 and 0.67 for p + Ag, p + Ta and p + ^{197}Au, respectively.

Although the fits displayed in fig. 6 are quite good, we notice that our model systematically fails to describe the yields of high-mass fragments ($A_F \to A_T$). This is indicative of *real physics*, since the purely statistical approach fails. Experimentally the high-mass fragments are produced by peripheral processes in which, for example, a few nucleons are "chipped off" the target leaving a large residual nucleus, or there is inelastic excitation and subsequent decay of the target. An impact-parameter independent p_B cannot be expected to describe such a production mechanism and we present an improvement in the next subsection.

As remarked on in the introduction, the suggestion that MFR explore liquid–gas phase-transition behavior[2]) led to increased interest in this type of reaction. In fig. 7 we show the data for p + Xe at 80–350 GeV taken by the Purdue Group[2]) together with fits according to both the phase-transition picture and the nuclear lattice model ($p_B = 0.82$). The two fits are equally good, with deviations from the data in the region $A_F \simeq 6$–10 being due to nuclear-structure effects. The fact that our model, despite its small physical content, can also describe this data, questions the validity of the liquid–gas phase-transition interpretation. Indeed, we have shown that this particular mass distribution is determined purely by simple statistics.

* Due to an erroneous fitting procedure, the constant-p_B fits to the same sets of data that were presented elsewhere[26,27]) are not quantitatively accurate.

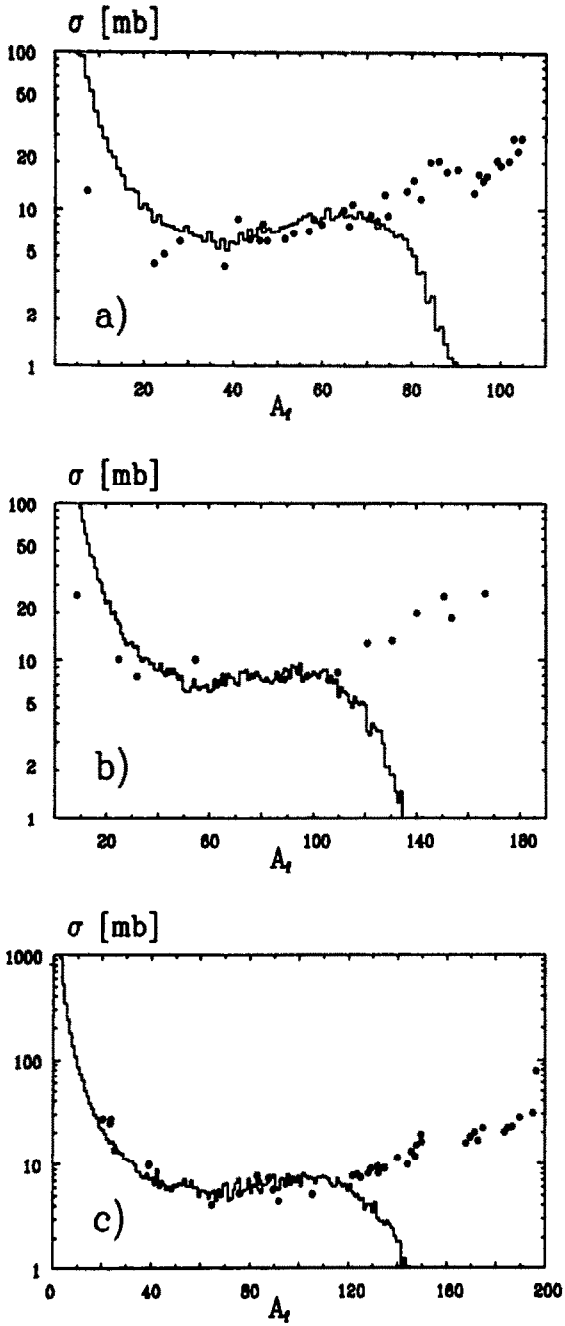

Fig. 6. Fits of NLM results to experimental data. (a) p + Ag at 11.5 GeV [ref. [23]], $p_B = 0.64$; (b) p + Ta at 5.7 GeV [ref. [24]], $p_B = 0.67$; and (c) p + ^{197}Au at 11.5 GeV [ref. [25]], $p_B = 0.67$.

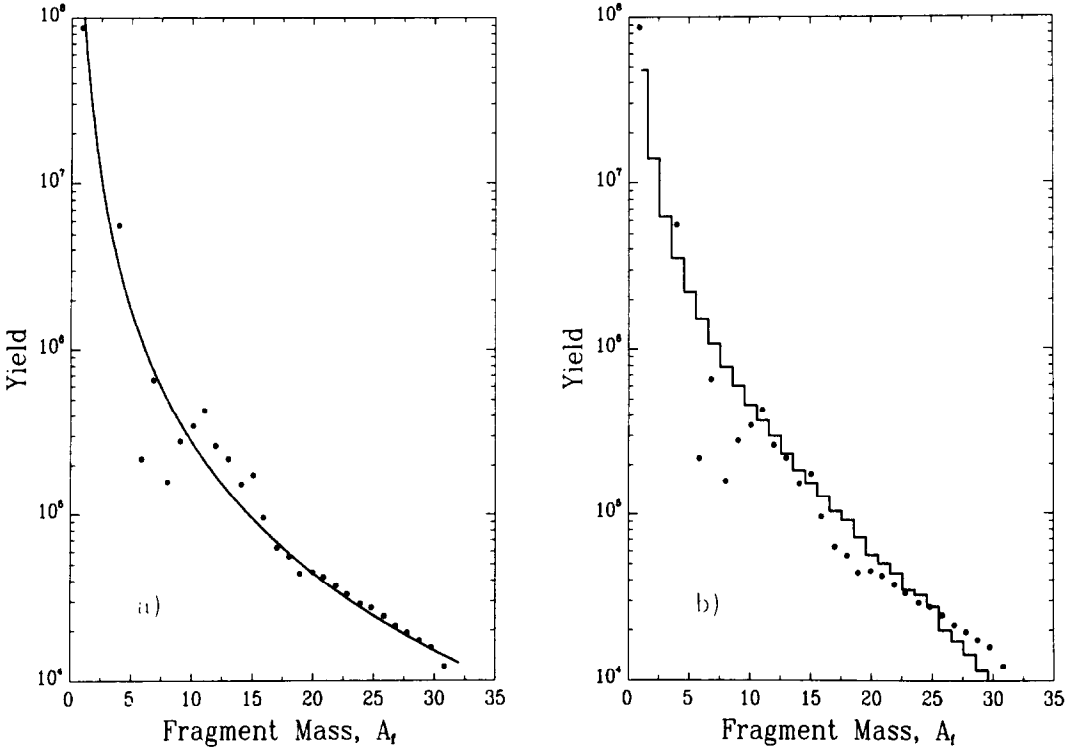

Fig. 7. For the reaction p + Xe at 80–350 GeV [ref.[2])] the data are fitted by (a) the phase-transition model, and (b) the NLM with $p_B = 0.82$.

The results of fig. 3 show that a given apparent exponent $\lambda > \tau$ corresponds to two possible values of p_B that are indistinguishable in the mass region where eq. (2.9) is valid. However, if heavy fragments are (are not) observed, one can immediately choose that p_B less (greater) than p_{BC}. In the p + Xe and p + Kr experiments[2]) it was *not feasible* to detect heavy fragments and so we apparently are left with an undetermined p_B: 0.58 *or* 0.82 for the xenon target and 0.58 or 0.81 in the case of krypton.

Evaluation of the *ratio* of the two experimental cross sections can, however, distinguish between these values. This is shown on the *left-hand* side of fig. 8, and we see that only the *higher* values of p_B describe the data correctly. Consequently, as these values of the breaking probability are greater than the critical one, these calculations imply that no high-mass fragments will be produced in these reactions. The excellent agreement between experiment and the NLM in this case is very encouraging. (The *right-hand* side of this figure is relevant to a later discussion.)

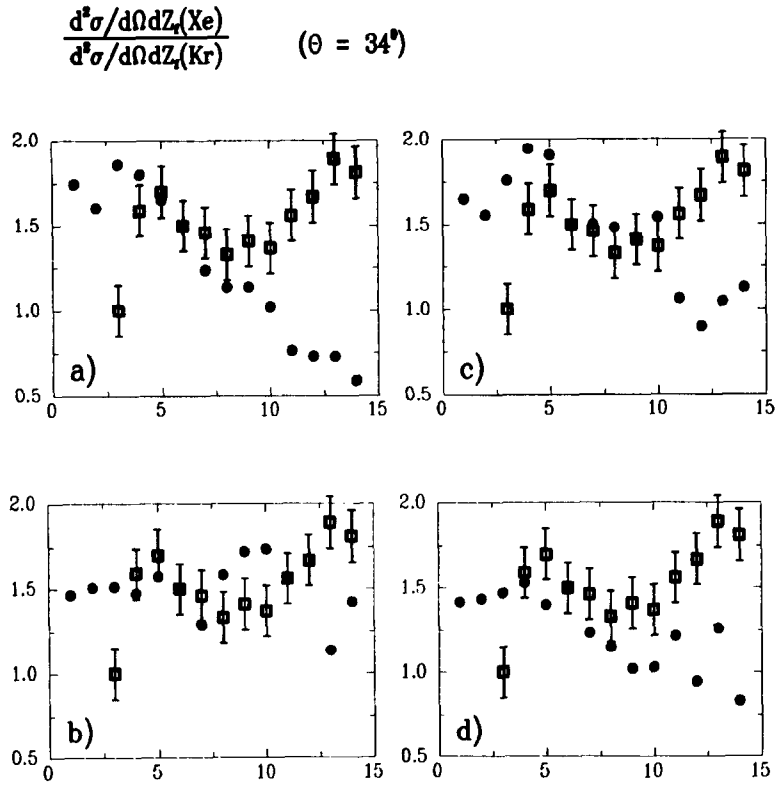

Fig. 8. The ratio of the yields in the p + Xe and p + Kr reactions at 80–350 GeV [refs.[2,15])]. The squares are the data points (with error bars) and the solid dots NLM results with: (a) Constant breaking probability, $p_B = 0.58$ and 0.58 (for Kr and Xe, respectively); (b) Constant breaking probability, $p_B = 0.81$ and 0.82 (Kr/Xe); (c) Woods-Saxon breaking probability, $p_{B0} = 0.62$ and 0.62 (Kr/Xe); (d) Woods-Saxon breaking probability, $p_{B0} = 0.88$ and 0.88 (Kr/Xe). Isospin symmetry was assumed in our calculation.

3.2. RELAXATION OF THE CONSTANT-p_B RESTRAINT

As stressed above, our initial aim when introducing the NLM was to provide a model that could be used to test different physical assumptions. This we now put into practice since, as we have seen in the previous section, a purely statistical model (p_B = constant) cannot reproduce all features of the data.

The energy deposited in the target by the projectile is larger for central than for grazing and distant collisions, and the breaking probability should reflect this. Assuming that this energy is deposited *uniformly* over the target, irrespective of b, we choose the simplest physically reasonable ansatz and write

$$p_B(b) = \frac{p_{B0}}{1 + \exp[(b - R)/a]}, \tag{3.1}$$

where p_{B0} is a normalization probability (or "central breaking probability") and R is the radius of the target nucleus. Since we do not know exactly how the energy is deposited, we leave the "diffuseness" a as a fit parameter.

We note that when $p_B(b) \neq$ constant, the physical size of the lattice constant, i.e. the spacing between lattice sites, must be specified. To do this we assume a bulk density equal to that of normal nuclear matter, $\rho_0 = 0.15$ nucleons/fm^3, and so obtain the relationship: 1 lattice constant $\simeq$ 1.9 fm. For our calculations we use

$$R = \left(\frac{3A}{4\pi}\right)^{1/3} \text{lattice constants} \simeq 1.2\ A^{1/3}\ \text{fm}. \tag{3.2}$$

We find that $a = 1.0$ fm is required to describe the data accurately.

In fig. 9 we fit the same data as in fig. 6 with the $p_B(b)$ of eq. (3.1). We find that $p_{B0} = 0.65$, 0.69 and 0.70 for p + Ag, p + Ta and p + ^{197}Au, respectively, and we see immediately that the quality of the fit is considerably better and the yields of both low- and high-mass fragments are described. Interestingly, for any given set of data, p_{B0} is greater than p_B. This is because the smaller breaking probability for non-central collisions causes a decrease in the production of light fragments which must be compensated for by a correspondingly larger breaking probability for central collisions, if the experimental yield of low-mass fragments is still to be reproduced. The production of small-to-medium mass fragments is dominated by central collisions and so it is clear that *complete* mass-yield distributions must be obtained if any meaningful clue to the underlying physics is to be found.

Applying the ansatz (3.1) to the p + Xe and p + Kr reactions gives values of p_{B0} of 0.62 or 0.88 for both sets of mass-yield data. Consideration of the cross-section ratio, however, *does not* enable us to choose a particular value of p_{B0}, since both give similar fits to data, as shown on the *right-hand* side of fig. 8. In this case multiplicity distributions would provide the actual p_{B0}, as $\langle m \rangle \simeq 10$ and 35 for $p_{B0} = 0.62$ and 0.88, respectively (Xe target).

We also tried different ansätze for $p_B(b)$ such as

$$p_B(b) = \begin{cases} p_{B0}\sqrt{\left[1 - (b/R)^2\right]} & (0 \leq b \leq R) \\ 0 & (b \geq R), \end{cases} \tag{3.3}$$

which can be derived, for example, from the number of primary nucleon-nucleon collisions suffered by the projectile as it crosses the target: clearly this depends on the impact parameter and the nucleon mean free path. However, this ansatz fails to reproduce the entire mass-yield distributions as well as eq. (3.1).

4. Multiplicity distributions and the apparent exponent

We found in sect. 2 that the apparent exponent λ, as defined by eq. (2.9), has a minimum value, equal to the critical exponent τ, at the percolation threshold

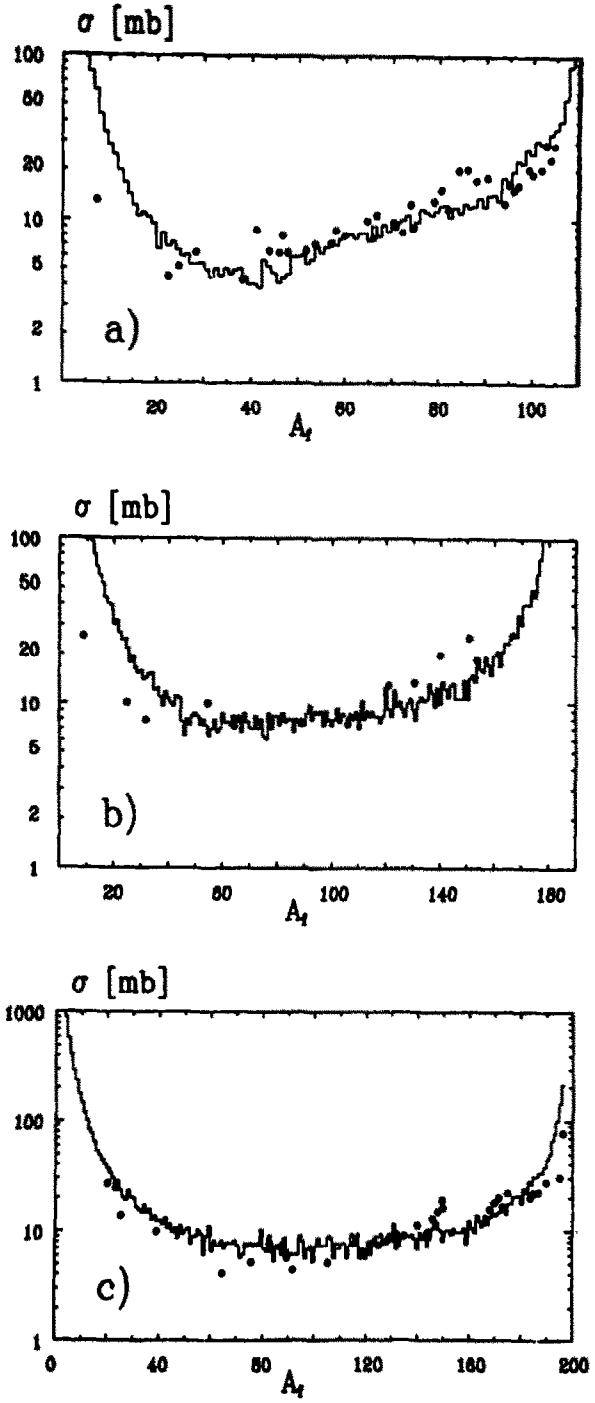

Fig. 9. The same as fig. 6 but with a Woods-Saxon ansatz for $p_B(b)$. (a) p + Ag at 11.5 GeV [ref.[23]], $p_{B0} = 0.65$; (b) p + Ta at 5.7 GeV [ref.[24]], $p_{B0} = 0.69$; and (c) p + ^{197}Au at 11.5 GeV [ref.[25]], $p_{B0} = 0.70$.

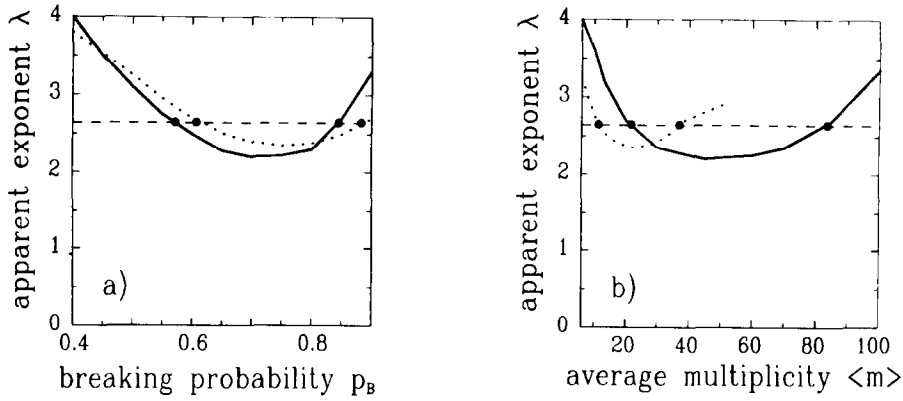

Fig. 10. The apparent exponent λ as a function of (a) p_B, and (b) the mean multiplicity $\langle m \rangle$ for the p + Xe system. The solid (dotted) curves are for a uniform (Woods-Saxon) breaking-probability distribution and the dots indicate the λ-values required to fit the mass-yield data.

specified by eq. (2.4). We also discovered that the mean fragment multiplicity $\langle m \rangle$ increases monotonically with increasing breaking probability, which was assumed to be constant over the entire lattice, and independent of the impact parameter. This monotonic increase allows elimination of the somewhat artificial quantity p_B and consequent construction of $\lambda(\langle m \rangle)$. For the p + Xe system the results are shown in fig. 10, with the solid points indicating the value of λ that fits the data (see fig. 7). Clearly a mean multiplicity measurement would, independently of the complementary p + Kr data, determine which of these two points is the physically relevant one, and hence the "true" value of p_B. In the previous section we took $p_B = 0.82$, equivalent to $\langle m \rangle \simeq 83$, as opposed to $p_B = 0.58$ ($\langle m \rangle \simeq 21$). As noted above, such a multiplicity measurement is necessary to determine the "true" value of p_{B0}.

In this figure we also show the behaviour of $\lambda(\langle m \rangle)$ for the ansatz (3.1) for $p_B(b)$. We see that in this case the mean multiplicities are much smaller for a given λ, because heavy fragments are inevitably produced. We see quite clearly that the correlation between λ and $\langle m \rangle$ is another tool that can be used to disentangle the physics of MFR. Unfortunately, to our knowledge no data exist at present which encompass both measurement of λ and $\langle m \rangle$.

Coming now to the discussion of the multiplicities alone we note a striking discrepancy between our results and those of Gross *et al.*[11]). They must specify the maximum allowable multiplicity *ab initio*, and, furthermore, must limit it to no more than 6 for computational reasons. Their resulting values of $\langle m \rangle$ are 3.0, 3.7 and 3.5 for p + Ag, p + Ta and p + ^{197}Au, respectively. However, as previously stated, the only free input to the NLM is p_B (or p_{B0}) and the multiplicity distribution is *automatically* obtained along with the mass yields. For the fits shown in sect. 3 (fig. 6) the calculated values of $\langle m \rangle$ are 27.7, 46.4 and 51.8 for p + Ag, p + Ta and

p + ^{197}Au, respectively, which are consistently about an order of magnitude greater than the results of ref.[11]). With the improvement of eq. (3.1) we obtain (for the fits shown in fig. 9) values for $\langle m \rangle$ of 12.0, 22.4 and 26.0 for p + Ag, p + Ta and p + ^{197}Au, respectively, which are also considerably larger than Gross's results. Similar multiplicities to ours have been calculated by Bondorf *et al.*[12]) using a thermodynamic approach.

5. Justification of the NLM and interpretation of p_B

In the previous sections we have seen that the nuclear lattice model can give a very good description of proton-induced MFR. It was also demonstrated that different physical processes can be incorporated within the model, as was initially hoped. Nonetheless, it was clear from the outset that the NLM has artificial features which lead one to question whether such a model can truly describe reality. However, somewhat paradoxically it seems that a *simple* description works *because* the process is complicated. The same is true in other areas of physics, good examples being flipping a coin or, as pointed out in ref.[1]), thermodynamics. We now intend to justify the model *a posteriori*.

As pointed out in sect. 2, results of SPT show that the presence of the lattice does not play a major role in determining cluster properties. We do, however, assume that the motion of the nucleons in the target can be neglected, or, in other words, that the projectile sees a frozen image of the target. This assumption is good for proton-induced collisions at the energies discussed in this paper, since the proton energy is much greater than the Fermi energy of the nucleons in the target. For heavy-ion projectiles one expects considerable distortions of the nuclear shape, perhaps coupled with high compressions, and then some re-consideration of the NLM becomes necessary. This will be done in the following section.

The model can also be criticized on the grounds that all possible partitions of the lattice are considered, without any allowance for, in particular, energy conservation. At the energies considered here, however, the proton has more than enough energy to break any reasonable nucleus into its constituent nucleons and energy conservation probably does not play an important role in determining the mass spectra. Underlying this statement is the assumption that the fragmentation is a fast, direct one-step process. In addition we note that it is not at all yet clear by what means energy is deposited in the spectators and consequently *how* energy conservation should be correctly formulated.

We do, however, conserve nucleon number and will also conserve charge when an isospin-dependent breaking probability is considered (see below).

The representation of complicated nucleon-nucleon interactions by only one parameter, the breaking probability, is, of course, a drastic simplification of reality and some link between these interactions, the excitation energy of the nucleus and p_B is required if the NLM is to be more than a sophisticated counting game. We

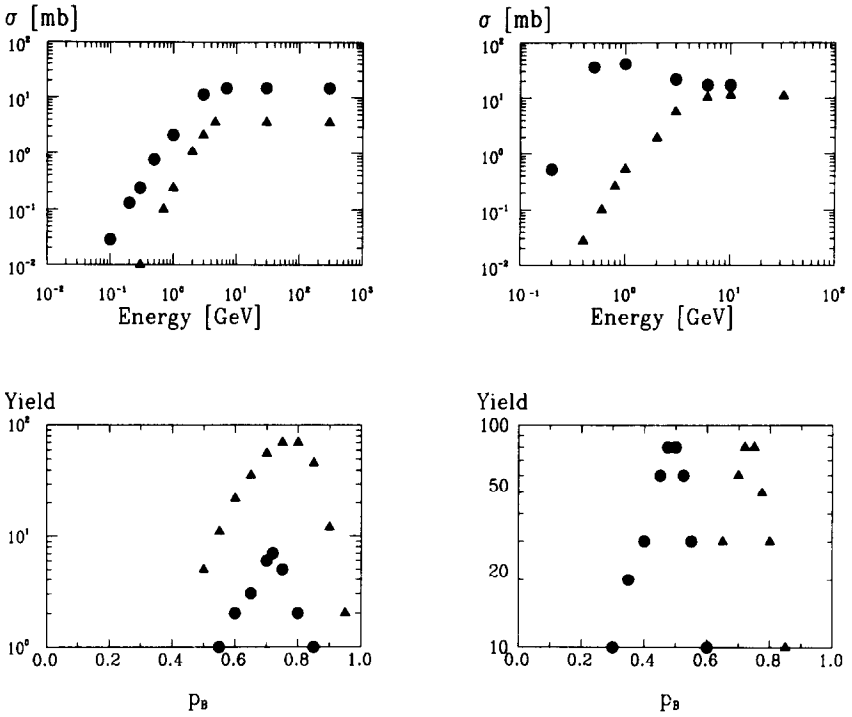

Fig. 11. Excitation functions for the production of (top left) ^{7}Be (dots) and ^{24}Na (triangles) in p + Ag reactions[28]), and (top right) ^{24}Na (triangles) and ^{175}Hf (dots) in p +^{197}Au reactions[28]). Note the saturation of the yields at higher incident energies. In the lower portions of the figure we show as a function of p_B the yields of (bottom left) mass-7 ("Be") (dots) and mass-24 ("Na") fragments (triangles) for a mass-107 ("Ag") target, and (bottom right) mass-24 ("Na") (triangles) and mass-175 ("Hf") fragments (dots) for a mass-197 ("Au") target. Comparison of the two left-hand figures and the two right-hand ones to each other, and reference to fig. 6, suggests that $0.64 \leq p_B^{max} \leq 0.72$ and $0.67 \leq p_B^{max} \leq 0.74$ for p + Ag and p +^{197}Au, respectively.

stress from the outset, though, that this is a far from trivial task and one that requires considerable investigation.

We begin by considering some data which have far-reaching consequences for our model. In fig. 11 we show excitation functions for the production of various fragments in the reactions p + Ag and p +^{197}Au. The data were gathered from ref.[28]) and references therein. We see, quite surprisingly, that the production cross sections for all types of fragment saturate above about 5 GeV incident proton energy and remain constant even when this energy is considerably greater. This can be interpreted as a limitation of the amount of energy that can be deposited in the target[1,14]). Naively, one expects the breaking probability to increase monotonically with increasing beam energy, but the results of fig. 11 imply that a limiting breaking

probability p_B^{max}, *smaller than unity*, is to be expected. This is an extremely important ingredient in the connection between the NLM and physics.

In the lower parts of fig. 11 we display the yields of various masses as a function of p_B for the p + Ag and p + Au systems. Clearly as $p_B \to 1$ these yields must vanish, which suggests, when due allowance is made for the mass-yield fits shown previously, that $0.64 \leq p_B^{max} \leq 0.72$ for p + Ag and $0.67 \leq p_B^{max} \leq 0.74$ for p + ^{197}Au.

With the $p_B(b)$ of eq. (3.1) the nucleus is not, on average, completely broken up for $p_{B0} \to 1$ and the corresponding limits on p_{B0}^{max} are $0.65 \leq p_{B0}^{max} \leq 0.85$ for p + Ag and $0.70 \leq p_{B0}^{max} \leq 0.75$ for p + ^{197}Au.

The data of ref.[2]) suggest that $p_B^{max} \simeq 0.81$ and 0.82 for p + Kr and p + Xe, respectively, since the fragment yields remain essentially constant for proton energies between 80 and 350 GeV.

We turn now to particular calculations of the breaking probability.

The cold-fragmentation picture of MFR, in which the spectator matter remains essentially cold and then breaks up, rather like the shattering of glass under impact, due to internal stresses or hydrodynamical instabilities at the participant-spectator boundary, has been quite successful[13,15]). In this picture Hüfner[29]) obtains a typical value for the breaking probability of about 0.6, in qualitative agreement with our fits to the data.

In this context we would like to note again that implicit in all our calculations has been the assumption of a cold fragmentation, i.e. a direct reaction. The other extreme is that of using a thermodynamic approach[11,12]). In this case the effects of the final state phase space become important and have to be taken into account.

In such a framework it is also possible to make an analogy between the NLM and the Ising model of ferromagnets[5]). It can then be shown[21,30]) that the temperature dependence of the breaking probability is

$$p_B = \exp\left[-E_B(T)/T\right], \tag{5.1}$$

where $E_B(T)$ is the energy required to break each bond (i.e. one-third of the binding energy per particle in an infinite simple-cubic system). In the Fermi-gas model at low temperatures

$$E_B(T) \simeq 16 - \tfrac{1}{16}T^2, \tag{5.2}$$

whereas for real nuclei (also at low temperatures)[3])

$$E_B(T) \simeq 8 - \tfrac{1}{8}T^2. \tag{5.3}$$

Assuming that the limiting excitation energy of nuclei is about 5 MeV/A [refs.[1,14]), eqs. (5.2) and (5.3) give values of p_B^{max} of 0.66 and 0.85, respectively. The results of Bonche *et al.*[4]) correspond to $p_B^{max} \simeq 0.89$–0.95, depending on the force used,

whereas Dean and Mosel suggest[5]), also on the basis of a thermal model, that $p_B^{max} \simeq 0.84$. All these values lie in the right "ballpark" and, interestingly, they are all close to the critical breaking probability. This could be one reason for the apparent success of the phase-transition model of MFR.

As previously noted, the apparent exponent λ, defined by eq. (2.9), has a minimum value equal to the critical exponent τ when $p_B = p_{BC}$ (see fig. 3). Since the same is true for a system undergoing a thermal phase transition at the critical point, Panagioutou *et al.*[31]) claim that the critical temperature T_C can be extracted from the available data. They suggest that λ has a minimum at $T = T_C \simeq 12$ MeV. The extraction of temperatures from data is, however, very difficult and subject to considerable interpretational problems[11,32]) and, perhaps more seriously, the results of classical molecular-dynamical calculations[6]) indicate that the critical region itself *cannot* be probed by MFR. Consequently, it would be unwise to use this procedure to determine the functional dependence $p_B(T)$. We simply note once more than $\lambda(p_B)$ and $\lambda(p_{B0})$ display minima *independent* of any thermodynamical input.

6. Conclusions and outlook

We have presented a tool with which different aspects of proton-induced MFR can be investigated. With only the simplest of assumptions we obtain an excellent description of the mass-yield curves, in particular their U-shape and $1/A_F^{\lambda}$ dependence for small-to-medium masses.

The connection with SPT has also been shown, and possible relationships to real physics of our only free parameter, the breaking probability, have been described. This parameter does not seem to vary very significantly from one system to another.

We have also demonstrated the importance of multiplicity measurements and complete mass-yield distributions. The relationship between multiplicity and apparent exponent is a particularly sensitive test of the physics of MFR, but suitable data is unfortunately lacking.

If, however, the NLM is to be more widely applicable, it must be extended to include heavy-ion reactions and to allow for a description of energy-related observables such as the energy spectra of the fragments. To calculate the latter it might be possible to allow the fragments to move apart from each other under the influence of their mutual Coulomb repulsion. It would be necessary, however, to work in a six-dimensional phase-space, with the momentum distribution of the particles introduced *ab initio*. This distribution could be taken from an appropriately calculated Wigner function, which would then also account for the Pauli principle[14]). It is important to note that such a version of the NLM would differ from $d = 6$ SPT insofar that the uncertainty principle implies that the position and momentum coordinates of the particles are not independent variables. Work in this direction is underway.

Another energy-related question is that of excited-fragment production and subsequent de-excitation. In the version of the NLM described in this paper all clusters generated are allowed, whether they are approximately spherical, cylindrical ("spaghetti" clusters), planar ("lasagne" clusters) or have more complicated non-compact shapes. In principle only the roughly spherical clusters should be detectable; the others should be allowed to de-excite, that is, be split into smaller, more compact clusters. The rms cluster radius and the ratio of surface area to volume could be among appropriate criteria for this subsequent division. As percolation theory shows that clusters are ramified for $p_B > p_{BC}$ [ref.[17])], many highly deformed "nuclei" will be formed for p_B close to p_B^{max}, which may be of particular importance for the p + Xe and p + Kr systems. We intend to investigate the effects of subsequent de-excitation in future work.

For a simple-cubic lattice, as used in the NLM, the number of nearest neighbours is six, whereas the α-particle, with no more than 3 bonds per nucleon, is the most stable composite nucleus. In connection with this and the known saturation properties of the nucleon-nucleon interation, it may be possible to use the idea of percolation with restricted valence[33]). Here occupation of a site or existence of a bond is prohibited if it leads to a site being connected to too many neighbouring sites. The effects of this in the nuclear case are worthy of investigation, as restricted valence seems to lead to a different percolation threshold[33]).

Not unrelated to the restricted-valence problem is consideration of the spin and, perhaps more importantly, the isospin dependence of the nucleon-nucleon interaction. It would be entirely possible to allow p_B to depend on the spin and isospin states of the nucleons, thus permitting calculation of isotopic distributions.

We feel that study of heavy-ion MFR should and can only be made concurrently with investigation of momentum-dependent effects. The reason for this lies in the belief that such reactions involve deformations and compressions very much larger than those expected with a proton projectile. How two heavy ions deform and respond to each other at these energies is not entirely understood, but the field is both fruitful and expanding. If such studies can provide a phase-space distribution of the nucleons, then this could be a useful starting point for a heavy-ion version of the NLM.

In addition, a combination of bond and site percolation could be used in a description of heavy-ion reactions, with the site-occupation probability being related to the density of the system and the bond-breaking probability to its temperature. A phase diagram, similar to that used in other applications of percolation theory[21,30]), could then be constructed.

To conclude, we stress once more that the nuclear lattice model is an extremely powerful and versatile tool for investigating *different* physical mechanisms within the *same* approach. Encouraged by the results presented here and stimulated by the possible extensions discussed above, we hope that further use of the NLM will elucidate the physical processes occurring during a multi-fragmentation reaction.

Appendix

We describe in this appendix the algorithm used for the counting of the clusters.

Let us denote the set of all grid points in an $n \times n \times n$ cube by A and by $A^{(0)} \leq A$ the subset of sites occupied by uncounted "nucleons". We note that for each member of A only one flag is required to indicate either whether it belongs to $B = A - A^{(0)}$ or to an already-counted cluster. Initially bonds are assumed to exist between all neighbouring pairs of sites belonging to this subset. These bonds are then "broken" with a probability p_B, and the problem is to "detect" and measure the size of the clusters so produced.

We scan A until the first point belonging to $A^{(0)}$ is found. This we denote by P_1, and we must now find all the other points of $A^{(0)}$ connected by unbroken bonds to P_1. We call $C^{(0)} = \{P_1\}$ the zeroth generation of C, where $C = \{P_1, \ldots, P_m\}$ represents all the sites of the cluster (of size m), of which P_1 is a member. All sites neighbouring P_1 and belonging to $A^{(1)} = A^{(0)} - C^{(0)}$ are then examined and those connected to P_1 by unbroken bonds form $C^{(1)}$. In general the nth generation of C, $C^{(n)}$, consists of all those points of $A^{(n)} = A^{(n-1)} - C^{(n-1)}$ which are connected via bonds to at least one point of $A^{(n-1)}$. This procedure is repeated until $C^{(n)} = \{\ \}$, and the total cluster is then given by

$$C = \bigcup_{i=0}^{n} C^{(i)}.$$

We illustrate our algorithm in fig. 12 for a square lattice. The different generations of C for $P_1 = (1,2)$ are

$$C^{(0)} = \{(1,2)\},$$
$$C^{(1)} = \{(2,2)\},$$
$$C^{(2)} = \{(2,1),(3,2)\},$$
$$C^{(3)} = \{(3,1),(3,3),(4,2)\},$$
$$C^{(4)} = \{(4,1),(4,3)\},$$
$$C^{(5)} = \{\ \}$$

and C is then a size-9 cluster.

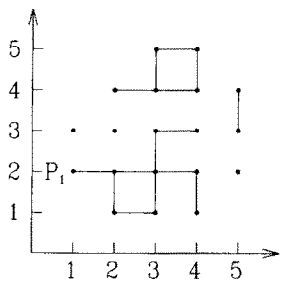

Fig. 12. Illustration of the cluster-counting algorithm for a square lattice. The occupied sites are indicated by dots and the unbroken bonds by solid lines.

The algorithm is then continued with a new starting point, P_1^{new}, that belongs to $A^{(0),\text{new}} = A^{(0)} - C$ until $A^{(0),\text{new}} = 0$.

References

1) J. Hüfner, Phys. Reports, to appear
2) R.W. Minich, S. Agarwal, A. Bujak, J. Chuang, J.E. Finn, L.J. Gutay, A.S. Hirsch, N.T. Porile, R.P. Scharenberg, B.C. Stringfellow and F. Turkot, Phys. Lett. **118B** (1982) 458;
A.S. Hirsch, A. Bujak, J.E. Finn, L.J. Gutay, R.W. Minich, N.T. Porile, R.P. Scharenberg, B.C. Stringfellow and F. Turkot, Phys. Rev. **C29** (1984) 508
3) G. Sauer, H. Chandra and U. Mosel, Nucl. Phys. **A264** (1976) 221;
H.R. Jaqaman, A.Z. Mekjian and L. Zamick, Phys. Rev. **C27** (1983) 2782;
A.L. Goodman, J.I. Kapusta and A.Z. Mekjian, Phys. Rev. **C30** (1984) 851
4) H.R. Jaqaman, A.Z. Mekjian and L. Zamick, Phys. Rev. **C29** (1984) 2067;
P. Bonche, S. Levit and D. Vautherin, Nucl. Phys. **A427** (1984) 278; **A436** (1985) 265;
S. Levit and P. Bonche, Nucl. Phys. **A437** (1985) 426
5) D.R. Dean and U. Mosel, Proc. 23rd Int. Winter Meeting on nuclear physics, Bormio, 1985, p. 798
6) A. Vicentini, G. Jacucci and V.R. Pandharipande, Phys. Rev. **C31** (1985) 1783
7) E.M. Lifshitz and L.P. Pitaevskii, Statistical physics (Pergamon, Oxford, 1980);
W. Thirring, Quantenmechanik grosser Systeme (Springer, Vienna, 1980)
8) W.A. Friedman and W.G. Lynch, Phys. Rev. **C28** (1983) 16, 950
9) B. Strack and J. Knoll, Z. Phys. **A315** (1984) 249;
J. Knoll, Proc. Seventh High-energy Heavy-ion Study, GSI Darmstadt, 1984, p. 741
10) J. Randrup and S.E. Koonin, Nucl. Phys. **A356** (1981) 223;
J. Randrup and G. Fai, Phys. Lett. **115B** (1982) 281;
G. Fai and J. Randrup, Nucl. Phys. **A381** (1982) 557; **A404** (1983) 551
11) D.H.E. Gross, L. Satpathy, Meng Ta-Chung and M. Satpathy, Z. Phys. **A309** (1982) 41;
D.H.E. Gross, Nucl. Phys. **A428** (1984) 313c;
Sa Ban-Hao and D.H.E. Gross, Nucl. Phys. **A437** (1985) 643
12) J.P. Bondorf, R. Donangelo, I.N. Mishustin, C. Pethick and K. Sneppen, Phys. Lett. **150B** (1985) 57;
J.P. Bondorf, R. Donangelo, K. Sneppen and H. Schulz, Proc. Informal Workshop on liquid–gas phase transitions in nuclei, Niels Bohr Institute, Copenhagen, 1985
13) J. Aichelin, H. Hüfner and R. Ibarra, Phys. Rev. **C30** (1984) 107
14) X. Campi, J. Desbois and E. Lipparini, Phys. Lett. **138B** (1984) 353; **142B** (1984) 8; Nucl. Phys. **A428** (1984) 327c;
X. Campi and J. Desbois, Proc. 23rd. Int. Winter Meeting on nuclear physics, Bormio, 1985, p. 497
15) J. Aichelin and J. Hüfner, Phys. Lett. **136B** (1984) 15
16) L.G. Sobotka and L.G. Moretto, Phys. Rev. **C31** (1985) 668
17) D. Stauffer, Phys. Reports **54C** (1979) 1;
J.W. Essam, Rep. Prog. Phys. **43** (1980) 883
18) W. Bauer, D.R. Dean, U. Mosel and U. Post, Phys. Lett. **150B** (1985) 53
19) G. Baym, Physica **96A** (1979) 131
20) J.W. Essam, in Phase transitions and critical phenomena, ed. C. Domb and M.S. Green (Academic, London, 1972) vol. 2, p. 192
21) A. Coniglio, H.E. Stanley and W. Klein, Phys. Rev. Lett. **42** (1979) 518;
D.W. Hermann and D. Stauffer, Z. Phys. **B44** (1981) 339
22) M.E. Fisher, Physics **3** (1967) 255; Proc. Int. School of Physics "Enrico Fermi", course LI, 1970, p. 1
23) G. English, N.T. Porile and E.P. Steinberg, Phys. Rev. **C10** (1974) 2268
24) J.R. Grover, Phys. Rev. **126** (1962) 1540
25) S.B. Kaufman, M.W. Weisfield, E.P. Steinberg, B.D. Wilkins and D. Henderson, Phys. Rev. **C14** (1976) 1121
26) W. Bauer, D.R. Dean, U. Mosel and U. Post, Proc. Seventh High-energy Heavy-ion Study, GSI Darmstadt, 1984, p. 701

27) W. Bauer, D.R. Dean, U. Mosel and U. Post, Proc. 23rd Int. Winter Meeting on nuclear physics, Bormio, 1985, p. 432
28) S.B. Kaufman and E.P. Steinberg, Phys. Rev. **C22** (1980) 167;
R.E.L. Green and G. Korteling, Phys. Rev. **C22** (1980) 1594
29) J. Hüfner, private communication
30) K. Binder and D. Stauffer, in Application of the Monte-Carlo Method in Statistical Physics, ed. K. Binder (Springer, Heidelberg, 1984) p. 241
31) A.D. Panagioutou, M.W. Curtin, H. Toki, D.K. Scott and P.J. Siemens, Phys. Rev. Lett. **52** (1984) 496;
A.D. Panagioutou, M.W. Curtin and D.K. Scott, Phys. Rev. **C31** (1985) 55
32) D.H. Boal, Phys. Rev. **C30** (1984) 119
33) J. Kertesz, B.K. Chakrabarti and J.A.M.S. Duarte, J. of Phys. **A15** (1982) L13